Cell Reports Medicine, Volume *5*

Supplemental information

Single-cell multiomics profiling reveals heterogeneous transcriptional programs and microenvironment in DSRCTs

Clémence Henon, Julien Vibert, Thomas Eychenne, Nadège Gruel, Léo Colmet-Daage, Carine Ngo, Marlène Garrido, Nicolas Dorvault, Maria Eugenia Marques Da Costa, Virginie Marty, Nicolas Signolle, Antonin Marchais, Noé Herbel, Asuka Kawai-Kawachi, Madison Lenormand, Clémence Astier, Roman Chabanon, Benjamin Verret, Rastislav Bahleda, Axel Le Cesne, Fatima Mechta-Grigoriou, Matthieu Faron, Charles Honoré, Olivier Delattre, Joshua J. Waterfall, Sarah Watson, and Sophie Postel-Vinay

Figure S1

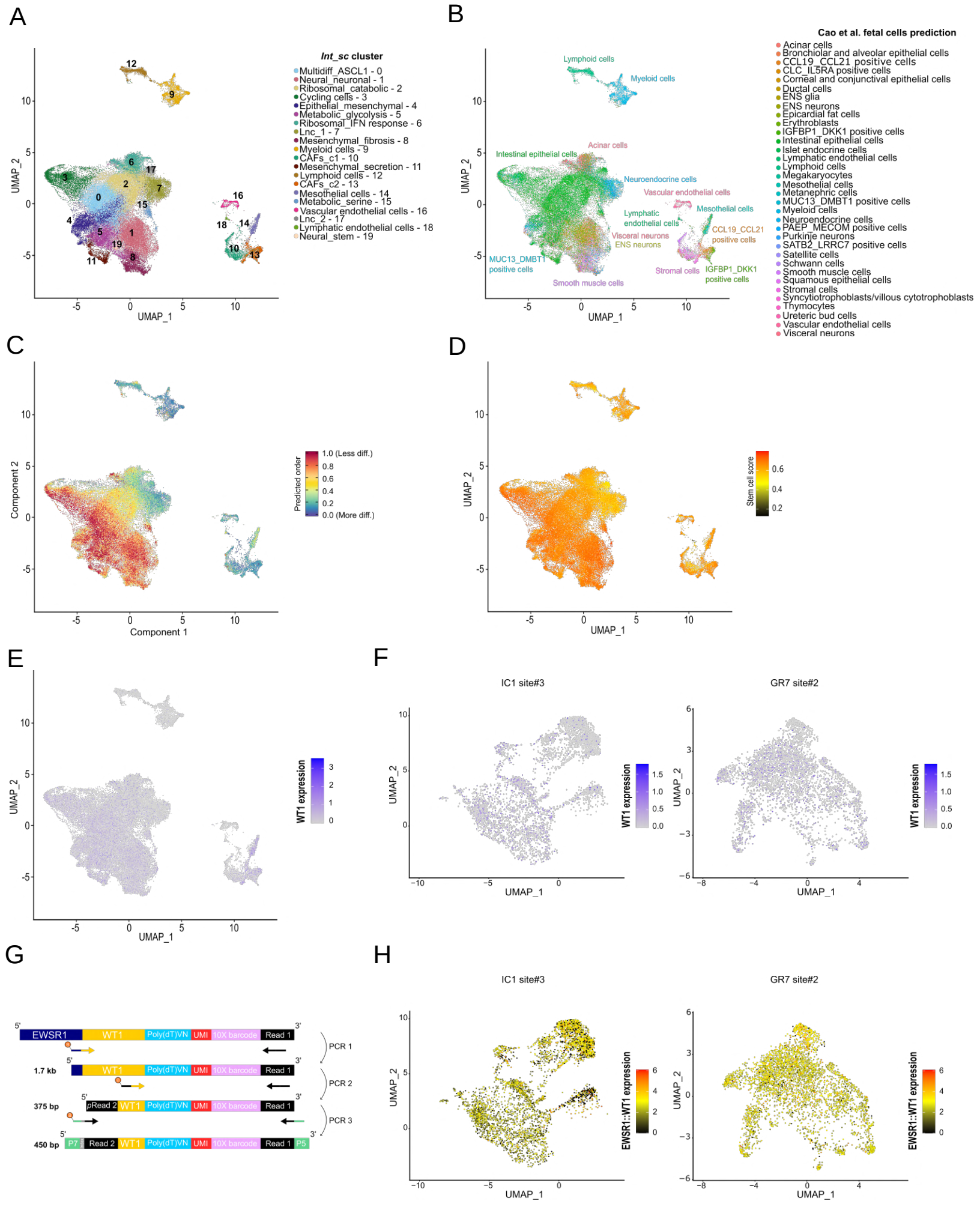
A
B
C
D
E
F
G
H
Int_sc cluster
Multidiff_ASCL1 - 0
Neural_neuronal - 1
Ribosomal_catabolic - 2
Cycling cells - 3
Epithelial_mesenchymal - 4
Metabolic_glycolysis - 5
Ribosomal_IFN response - 6
Lnc_1 - 7
Mesenchymal_fibrosis - 8
Myeloid cells - 9
CAFs_c1 - 10
Mesenchymal_secretion - 11
Lymphoid cells - 12
CAFs_c2 - 13
Mesothelial cells - 14
Metabolic_serine - 15
Vascular endothelial cells - 16
Lnc_2 - 17
Lymphatic endothelial cells - 18
Neural_stem - 19
Cao et al. fetal cells prediction
Acinar cells
Bronchiolar and alveolar epithelial cells
CCL19_CCL21 positive cells
CLC_IL5RA positive cells
Corneal and conjunctival epithelial cells
Ductal cells
ENS glia
ENS neurons
Epicardial fat cells
Erythroblasts
IGFBP1_DKK1 positive cells
Intestinal epithelial cells
Islet endocrine cells
Lymphatic endothelial cells
Lymphoid cells
Megakaryocytes
Mesothelial cells
Metanephric cells
MUC13_DMBT1 positive cells
Myeloid cells
Neuroendocrine cells
PAEP_MECOM positive cells
Purkinje neurons
SATB2_LRRC7 positive cells
Satellite cells
Schwann cells
Smooth muscle cells
Squamous epithelial cells
Stromal cells
Syncytiotrophoblasts/villous cytotrophoblasts
Thymocytes
Ureteric bud cells
Vascular endothelial cells
Visceral neurons
Lymphoid cells
Myeloid cells
Acinar cells
Intestinal epithelial cells
Neuroendocrine cells
Vascular endothelial cells
Mesothelial cells
Lymphatic endothelial cells
CCL19_CCL21 positive cells
Visceral neurons
ENS neurons
MUC13_DMBT1 positive cells
Stromal cells
IGFBP1_DKK1 positive cells
Smooth muscle cells
UMAP_1
UMAP_2
Component 1
Component 2
Predicted order
1.0 (Less diff.)
0.8
0.6
0.4
0.2
0.0 (More diff.)
Stem cell score
WT1 expression
IC1 site#3
GR7 site#2
EWSR1
WT1
Poly(dT)VN
UMI
10X barcode
Read 1
Read 2
P7
P5
1.7 kb
375 bp
450 bp
PCR 1
PCR 2
PCR 3
EWSR1::WT1 expression

Figure S1. DSRCTtumor cells are characterized by lineage-related states, stemness features, and homogeneous EWSR1::WT1 expression levels, related to Figures 1 and 2.

(A) Uniform Manifold Approximation and Projection (UMAP) highlighting *Int_sc* 3' scRNA-seq clusters.
(B) UMAP showing the *Int_sc* dataset annotation according to Cao et al. fetal cells atlas.
(C) UMAP highlighting differentiation degree prediction of the *Int_sc* dataset using CytoTRACE.
(D) UMAP showing cell-based transcriptome entropy of the *Int_sc* dataset using StemID.
(E) UMAP showing "WT1" expression within *Int_sc* dataset. "WT1" herein corresponds to both EWSR1::WT1 and wild-type WT1 transcripts.
(F) UMAP showing "WT1" expression within IC1 site#3 (left panel) and GR7 site#2 (right panel) datasets.
(G) Schematic representation of the in-house developed method characterizing EWSR1::WT1 fusion transcript expression level at the single-cell resolution. The method relies on sequential PCRs to enrich the library for EWSR1::WT1 specific barcoded cDNAs derived from 10X Genomics 3' single cell pipeline.
(H) UMAP highlighting EWSR1::WT1 single-cell expression level in IC1 site#3 and GR7 site#2.

Figure S2

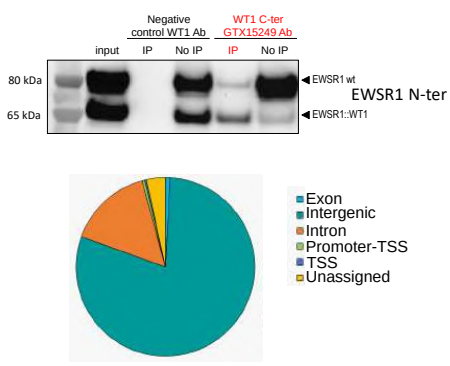

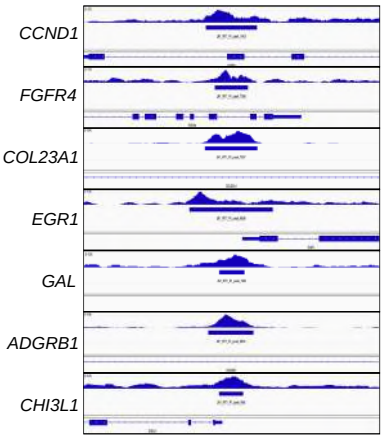

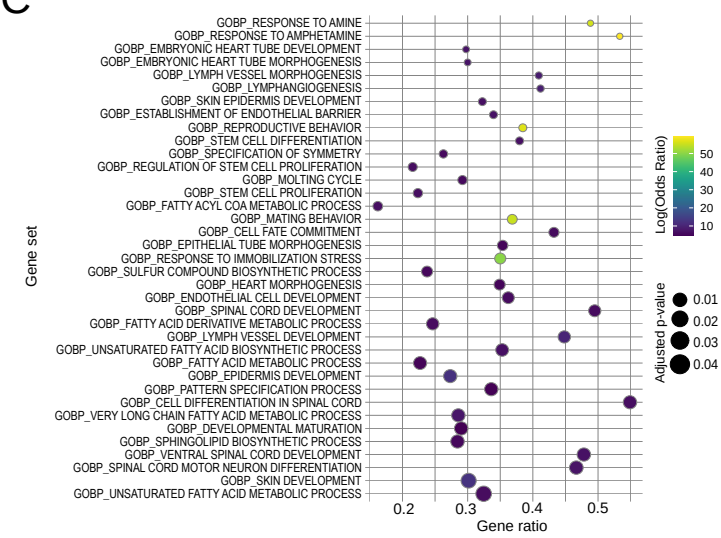

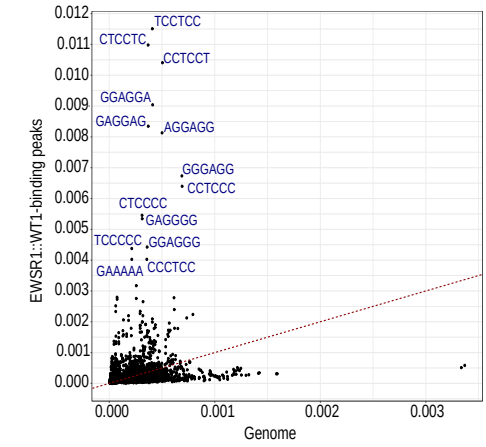

E

Rank	De novo motif ID	Logo	Best match JASPAR2020	Best match HOCOMOCO-v11
Rank 1	m1_GCGKGGGAGGVRGV		EGR1 [RC]	WT1+/-KTS
Rank 2	m5_CCCACGCA		EGR2	EGR2
Rank 3	m7_GGAGGAGRAGGAGAA		ZNF263	ZNF263
Rank 4	m2_GGAGGAGGAGRAAGA		ZNF263	ZNF263
Rank 5	m8_CCTCCTCCTCTTCC		ZNF263 [RC]	ZNF263 [RC]
Rank 6	m3_AARTAAAYA		FOXC2	FOXJ2
Rank 7	m4_GAGCCACTTCC		ZNF528	XBP1 [RC]
Rank 8	m6_ACCTGKCT		MYOD1	FIGLA [RC]

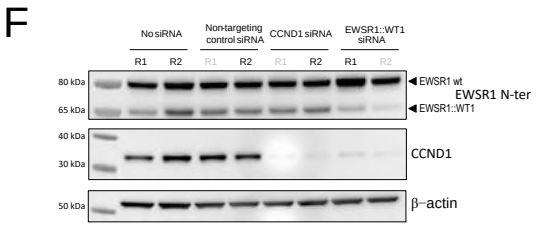

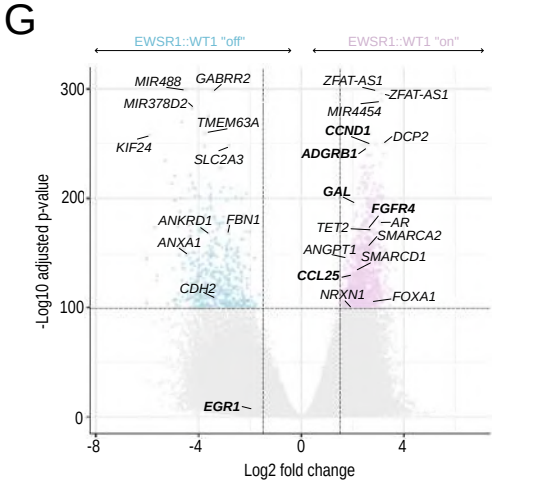

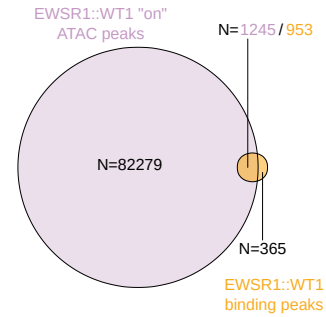

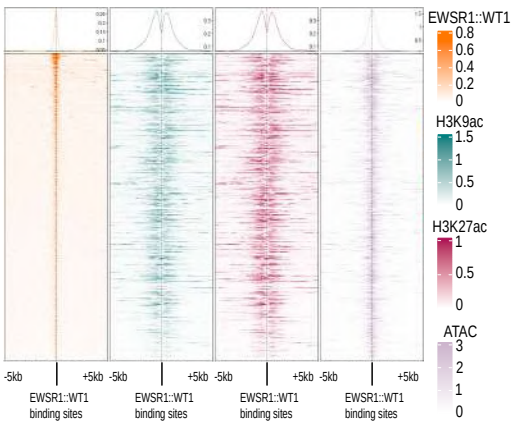

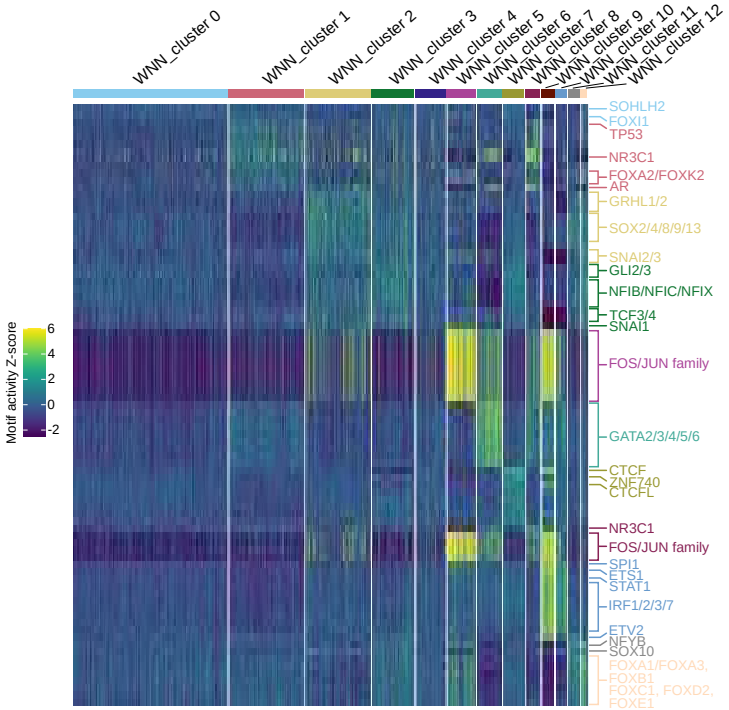

Figure S2. EWSR1::WT1 target genes display EGR1 motif and are variably accessible across snMultiome clusters, related to Figure 3.

(A) EWSR1 western blot (WB) showing the input, immunoprecipitated (IP), and flow-through fractions (No IP) of EWSR1::WT1 in JN-DSRCT-1 protein lysate (upper panel). IP was done using WT1 C-ter GTX15249 antibody. As a negative control, we show an inefficient immunoprecipitation with an alternate WT1 antibody. Strong staining for EWSR1 at the predicted fusion protein size (65 kDa) highlights the specificity of the immunoprecipitated fraction. WB was performed using the EWSR1 C-9 clone, sc-48404.
Pie chart representing the genomic distribution of EWSR1::WT1-binding peaks (lower panel). TTS relates to transcription termination site.
(B) Integrated Genome Viewer (IGV) track of EWSR1::WT1 known (*CCND1, FGFR4, COL23A1, EGR1*) and newly described (*GAL, ADGRB1, CHI3L1*) targets.
(C) Gene Ontology (GO) enrichment analysis of EWSR1::WT1-binding peaks for GO biological process (GOBP). All pathways with significant enrichment (adjusted p-value <0.05) are displayed on y-axis from lower (top) to higher (bottom) adjusted p-value. Gene ratio is shown on x-axis. Dots color refer to Log(Odds Ratio).
(D) Scatter plot representing 6-mers frequency within EWSR1::WT1-binding peaks (y-axis) according to their frequency within the whole genome (x-axis). Specific enrichment for GGA/CCT repeats motifs is highlighted.
(E) Chart recapitulating significantly enriched de novo EWSR1::WT1-binding motifs with their best match with known transcription factor (TF) consensus motifs. The analysis was performed using the MEME suite with JASPAR2020 or HOCOMOCO-v11 TF database.
(F) WB of EWSR1::WT1 expression assessment upon EWSR1::WT1 silencing of JN-DSRCT-1 cells before assay for transposase-accessible chromatin with sequencing (ATAC-seq). Silencing was performed using a EWSR1::WT1- or CCND1-targeting siRNA, or a control non-targeting siRNA at H48 post-transfection. A mock-transfected control is shown. EWSR1::WT1 and wild type EWSR1 correspond to the 65 kDa and 80 kDa band respectively, using a EWSR1 N-ter antibody (EWSR1 C-9 clone, sc-48404). CCND1, which is a direct target of EWSR1::WT1, is shown as a positive control for efficient EWSR1::WT1 silencing. b-actin is shown as a control for protein loading at 50 kDa.
(G) Volcano plot showing ATAC-seq differentially accessible peaks-corresponding genes in EWSR1::WT1-silenced versus non-silenced JN-DSRCT-1 cells. Peaks with increased accessibility upon EWSR1::WT1 silencing are shown on the left (EWSR1::WT1 “off”), whereas those that have increased accessibility in non-silenced cells are shown on the right (EWSR1::WT1 “on”). Colored dots correspond to the most differentially accessible peaks (-Log10(adjusted p-value)>100 and absolute Log2 fold change (Log2FC)>1.5).
(H) Venn diagram showing overlap between EWSR1::WT1 “on” ATAC peaks and EWSR1::WT1-binding peaks.
(I) ChIP-seq read coverage heatmaps centered around EWSR1::WT1-binding peaks (+/- 5 kb) and ordered by genomic regions. Heatmaps display EWSR1::WT1 (first panel), H3K9ac (second panel), and H3K27ac (third panel) ChIP-seq assays. The fourth panel shows coverage for EWSR1::WT1 “on” peaks from ATAC-seq assay.
(J) Heatmap showing cell-based motif activity Z-score for the top enriched motifs from known TFs in the snMultiome assay.

Figure S3

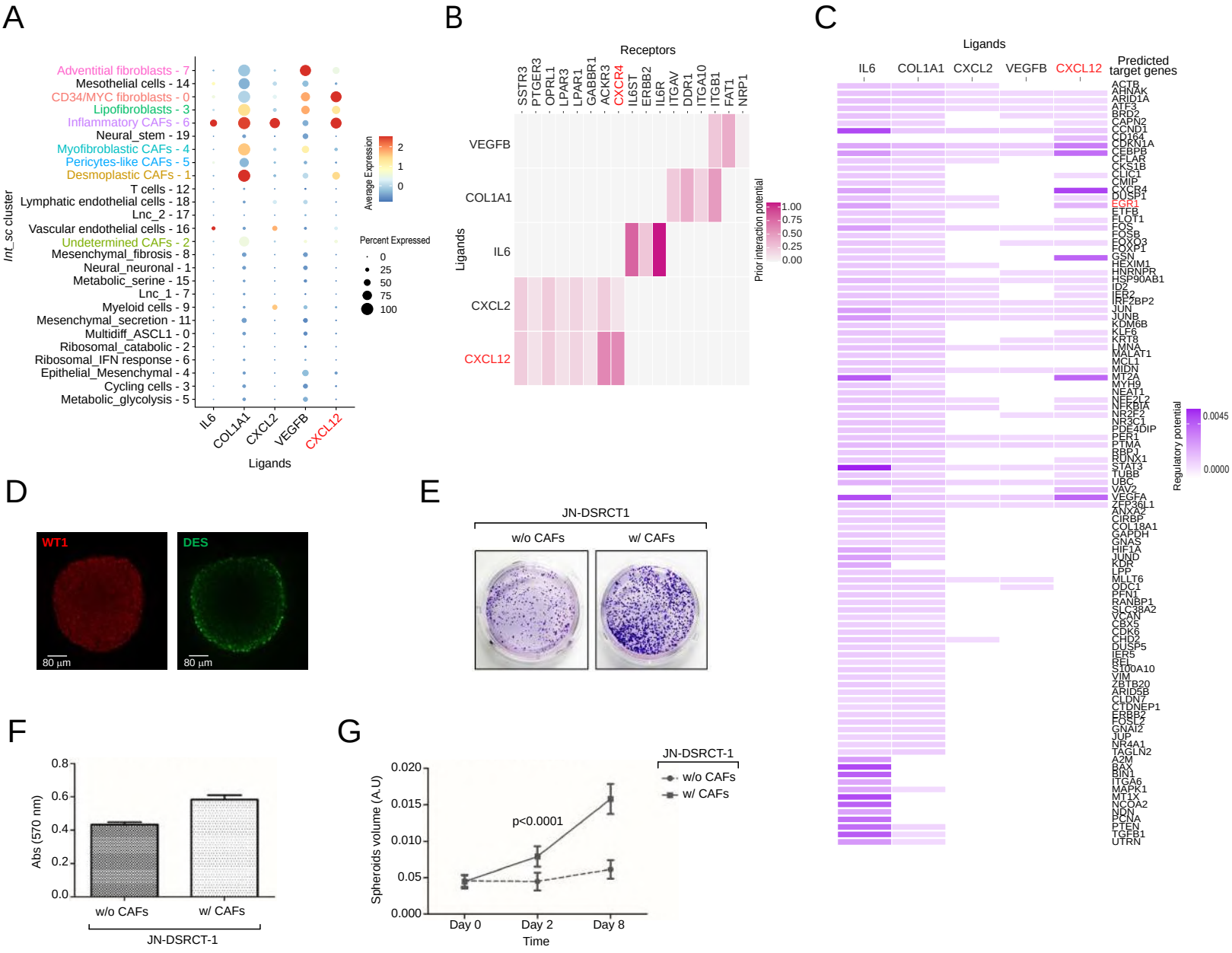
A
Adventitial fibroblasts - 7
Mesothelial cells - 14
CD34/MYC fibroblasts - 0
Lipofibroblasts - 3
Inflammatory CAFs - 6
Neural_stem - 19
Myofibroblastic CAFs - 4
Pericytes-like CAFs - 5
Desmoplastic CAFs - 1
T cells - 12
Lymphatic endothelial cells - 18
Lnc_2 - 17
Vascular endothelial cells - 16
Undetermined CAFs - 2
Mesenchymal_fibrosis - 8
Neural_neuronal - 1
Metabolic_serine - 15
Lnc_1 - 7
Myeloid cells - 9
Mesenchymal_secretion - 11
Multidiff_ASCL1 - 0
Ribosomal_catabolic - 2
Ribosomal_IFN response - 6
Epithelial_Mesenchymal - 4
Cycling cells - 3
Metabolic_glycolysis - 5
Int_sc cluster
IL6
COL1A1
CXCL2
VEGFB
CXCL12
Ligands
Average Expression
Percent Expressed
B
Receptors
SSTR3
PTGER3
OPRL1
LPAR3
LPAR1
GABBR1
ACKR3
CXCR4
IL6ST
ERBB2
IL6R
ITGAV
DDR1
ITGA10
ITGB1
FAT1
NRP1
Ligands
Prior interaction potential
C
Ligands
Predicted target genes
Regulatory potential
D
WT1
DES
80 µm
E
JN-DSRCT1
w/o CAFs
w/ CAFs
F
Abs (570 nm)
w/o CAFs
w/ CAFs
JN-DSRCT-1
G
JN-DSRCT-1
w/o CAFs
w/ CAFs
p<0.0001
Spheroids volume (A.U)
Day 0
Day 2
Day 8
Time

Figure S3. Microenvironment shapes DSRCT cells phenotype, related to Figure 5.

(A) Selected ligands expression across Int_sc dataset clusters (NichetNet). The color scale represents the average expression Z-score percluster. For each cluster, the percentage of cells expressing the feature of interest is represented by the dot size.
(B) Prior ligand-receptor interaction potential between selected ligands and matching receptors in the Int_sc dataset (NicheNet).
(C) Regulatory potential between selected ligands and imputed downstream target genes from high (purple) to low (white) regulatory activity.
(D) Representative image of a JN-DSRCT-1 spheroid embedded in Matrigel stained for DES and WT1.
(E) Colony formation assay (CFA) of JN-DSRCT-1 cell line cocultured with (w/) or without (w/o) CAFs obtained from DSRCT patients-derived xenografts (PDXs). The picture shows colonies stained with crystal violet after two weeks of coculture.
(F) Barplots showing the percentage of well area covered by JN-DSRCT-1 colonies cultures with (w/) or without (w/o) PDXs-derived CAFs, assessed by absorbance cell viability assay. A t-test was used for p-value calculation.
(G) JN-DSRCT-1 spheroids growth culture in the presence (w/) or absence (w/o) of DSRCT PDXs-derived CAFs. The median volume of the spheroids (triplicate assay) assessed at Day 0, Day 2, and Day 8 is shown on y-axis. A.U: Arbitrary Unit; two-way ANOVA was used for p-value calculation.